APPLIED PHYSICS

Completely foldable electronics based on homojunction polymer transistors and logics

Min Je Kim[1†], Hwa Sook Ryu[2†], Yoon Young Choi[1], Dong Hae Ho[1], Yoonjoo Lee[2], Ayushi Tripathi[2], Jae Hoon Son[2], Yeran Lee[2], Seunghan Kim[3], Moon Sung Kang[3,4], Han Young Woo[2]*, Jeong Ho Cho[1]*

An increase in the demand for completely foldable electronics has motivated efforts for the development of conducting polymer electrodes having extraordinary mechanical stability. However, weak physical adhesion at intrinsic heterojunctions has been a challenge in foldable electronics. This paper reports the completely foldable polymer thin-film transistors (PTFTs) and logic gate arrays. Homojunction-based PTFTs were fabricated by selectively doping p-type diketopyrrolopyrrole-based semiconducting polymer films with $FeCl_3$ to form source/drain electrodes. The doping process caused a gradual work function change with depth, which promoted charge injection to semiconducting regions and provided a low contact resistance. In addition, the interfacial adhesion in the PTFTs was improved by interfacial cross-linking between adjacent component layers. The electrical performance of the resulting PTFTs was maintained without noticeable degradation even after extreme folding, suggesting that the proposed fabrication strategy can further be applied to various semiconducting polymers for the realization of foldable electronics.

INTRODUCTION

The past decade has witnessed unprecedented advances in deformable electronics—from rudimentary flexible devices to bendable, rollable, and foldable devices—aimed at the satisfaction of increasing demands for device portability and usability (1–12). Because foldable electronics are required to have exceptionally high mechanical stability, the development of electrical components that can withstand extreme environments has become a critical task. Conventional metallic electrodes, such as copper, aluminum, silver, and gold electrodes, exhibit excellent electrical conductivity, but their rigidity and brittleness cause the device to be susceptible to interfacial delamination between device component layers (13–15); this problem hampers their application to foldable electronics. Conducting polymers, such as polypyrrole, polyaniline, and poly(3,4-ethylenedioxythiophene): poly(styrenesulfonate) (PEDOT:PSS), have been proposed and widely used as alternatives to conventional metallic electrodes because of their mechanical robustness (4, 7, 16, 17). These conducting polymers have several advantages over conducting metals, such as chemical versatility, flexibility, corrosion resistance, and adjustable conductivity (4, 7, 17–20). Although conducting polymers are an excellent platform for foldable electronics, achieving the requisite mechanical stability of the structure of an electronic device remains a challenging task. In general, an electronic device is composed of component layers, i.e., an electrode, semiconductor, and insulator, stacked on a substrate (21). The adhesion at the interfaces between these layers is affected by the repeated folding and unfolding of the device (16, 22, 23). The electrode/semiconductor interface has received more attention than the other interfaces because charge transport occurs across these layers (24, 25). Therefore, it is crucial to improve the mechanical stability of the electrode/semiconductor interface under physical deformation. However, studies conducted thus far for enhancing this mechanical stability have reached a dead end. This limitation on further improvement of mechanical stability is attributed to the widely known intrinsic drawback of the heterojunction interface between the electrode layer and the semiconductor layer (26, 27), whereby the quality of the interface itself depends solely on the strength of the physical adhesion. From this viewpoint, a homojunction is highly advantageous in that it makes the interface more stable and, consequently, more durable under extreme strain conditions such as folding (28, 29).

Here, we present a simple fabrication method for homojunction-based completely foldable polymer thin-film transistors (PTFTs) and logic gate arrays. The properties of the interface between the electrical components of a device should be improved to ensure durability of the device under extreme strain (e.g., folding) conditions. Here, the selective doping of the semiconducting polymer layer enables the successful formation of a homojunction between the semiconductor and the electrode as an alternative to existing heterojunction-based devices; this homojunction consequently improves the mechanical stability of the PTFTs. In addition, work function changes (with depth) in the doped regions as induced by the sequential doping promote efficient charge injection to (or from) the semiconducting region, and consequently, the contact resistance of the fabricated doped-semiconductor–based PTFTs is comparable to that of Au-electrode–based PTFTs, although the electrical conductivity and work function of the former are lower than those of the latter. Poor adhesion at the various component layer interfaces (e.g., the semiconductor/substrate and semiconductor/dielectric interfaces) is also remarkably improved by the interfacial cross-linking that occurs alongside the cross-linking within each layer, as is confirmed from the unchanged key parameters of the homojunction PTFTs; specifically, the carrier mobility, on-off current ratio, and turn-on voltage all show negligible degradation even after 2000 cycles of extreme bending strain. We believe that these foldable PTFTs and logic gates will drive innovation in industries related to foldable electronics.

[1]Department of Chemical and Biomolecular Engineering, Yonsei University, Seoul 03722, Republic of Korea. [2]Department of Chemistry, KU-KIST Graduate School of Converging Science and Technology, Korea University, Seoul 02841, Republic of Korea. [3]Department of Chemical and Biomolecular Engineering, Sogang University, Seoul 04107, Republic of Korea. [4]Institute of Emergent Materials, Sogang University, Seoul 04107, Republic of Korea.
*Corresponding author. Email: hywoo@korea.ac.kr (H.Y.W.); jhcho94@yonsei.ac.kr (J.H.C.)
†These authors contributed equally to this work.

RESULTS

Fabrication of completely foldable homojunction PTFTs

Figure 1A shows a schematic illustration of the concept of completely foldable PTFTs. For a foldable device to be able to operate stably over its expected lifetime of 5 years, it must endure 200,000 folding cycles (*30*); this requirement necessitates a completely foldable transistor backplane. The photographic image in the bottom-left corner of Fig. 1A shows the fabricated foldable transistor array. The factor that most severely hampers the achievement of this level of mechanical stability is the poor adhesion at the interfaces between the electrical components (the semiconductor, dielectric, and source/drain and gate electrodes) constituting the foldable transistor (*16*, *23*, *27*). The enhancement of the adhesion strength at interfaces is a great challenge to the realization of completely foldable electronic devices. Interfacial adhesion can be enhanced by the selective doping of the organic semiconductor (OSC) layer to induce the semiconductor-to-conductor transition for the realization of the source/drain polymer electrodes, which form a homojunction with the semiconducting channel in a PTFT architecture. Interfacial adhesion can be enhanced by the following two strategies, also illustrated in Fig. 1B. One is the selective doping of the OSC layer to form a homojunction between the semiconducting channel and the source/drain electrodes in a PTFT. In addition to forming the homojunction, this strategy induces a gradual change in the work function with depth, thereby promoting charge injection between the semiconducting layer and the source/drain electrode

layer; this is discussed in detail later in the paper. The other strategy for achieving the desirable mechanical properties of foldable electronics is interfacial cross-linking. The fabrication procedure of a completely foldable PTFT on a 12-μm-thick polyethylene terephthalate (PET) substrate is illustrated in Fig. 1C. First, a semiconductor film based on poly[2,5-(2-decyltetradecyl)-3,6-diketopyrrolopyrrole-alt-5,5-(2,5-di(thien-2-yl)thieno[3,2-b]thiophene)] (PDPPT-TT) was patterned on a PET substrate using ethylene 1,2-bis(4-azido-2,3,5,6-tetrafluorobenzoate) as a photocrosslinker (chemical structure as shown in fig. S1A) (*3*, *31*); this film functioned as both the semiconducting channel and the source/drain electrodes. Specifically, a mixture solution of PDPPT-TT and azide cross-linker in chlorobenzene (CB) was spin-coated onto the substrate and then selectively exposed to 254-nm ultraviolet (UV) light through a shadow mask. The cross-linking reaction in the presence of the azide cross-linker was confirmed by Fourier transform infrared spectroscopy; the characteristic vibration peak of the azide group (2125 cm^{-1}) disappeared completely after UV exposure, as shown in fig. S1B. The unexposed area was then removed by rinsing with CB solvent, which yielded a photopatterned PDPPT-TT layer. In the second step, the gate dielectric layer was formed via the photopatterning of a poly(methyl methacrylate) (PMMA) layer onto the patterned PDPPT-TT layer using azide cross-linker by the above-described method. Subsequently, the PDPPT-TT:azide cross-linker film was spin-coated and photopatterned onto the PMMA pattern. The detailed fabrication procedures of the completely foldable PTFTs are described in
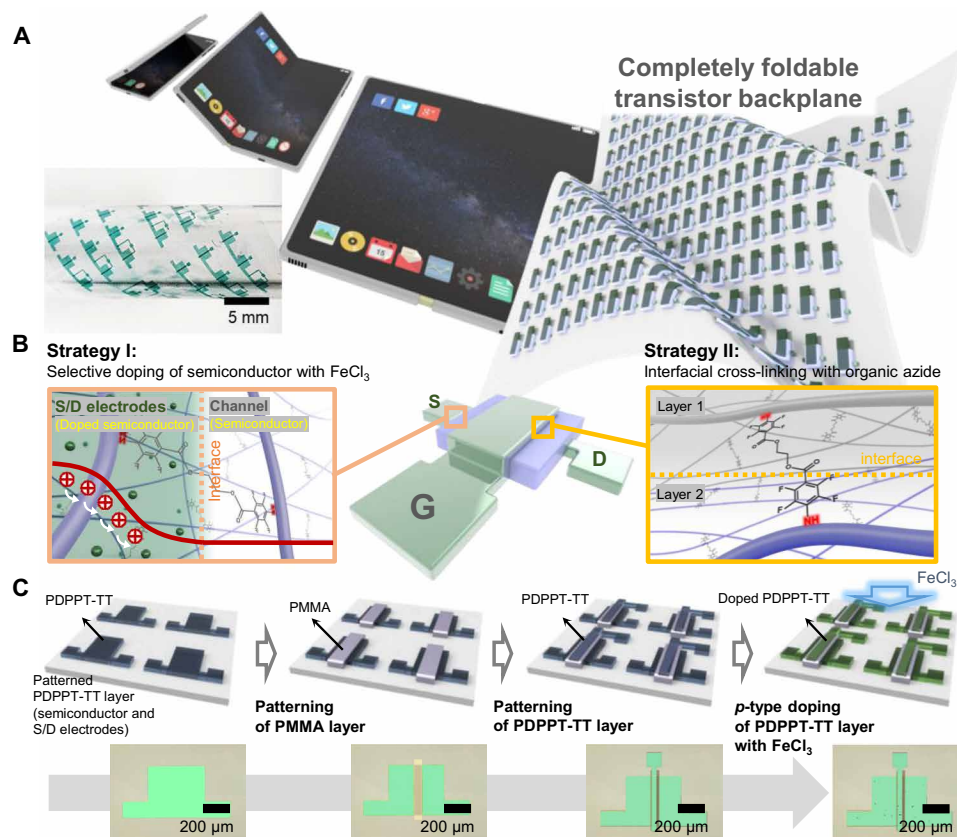

Fig. 1. Concept and fabrication of completely foldable homojunction PTFTs. (**A**) Schematic illustration and photographic image of completely foldable PTFT. (**B**) Two strategies for fabrication of completely foldable PTFTs. S/D/G, source/drain/gate. (**C**) Fabrication procedure of homojunction PTFTs.

Materials and Methods. Azide cross-linker not only induced a cross-linking reaction within the semiconducting or dielectric layer but also notably improved the interfacial adhesion by inducing interfacial cross-linking reactions between adjacent layers, i.e., at the substrate/OSC, OSC/PMMA, and PMMA/OSC interfaces (details provided below). Sequential doping was performed by coating FeCl$_3$ solution (in acetonitrile) onto the patterned PET/OSC/PMMA/OSC multilayer structure to selectively p-dope the PDPPT-TT source, drain, and gate electrode regions simultaneously (32, 33). It should be noted that the capacitive property of the cross-linked PMMA was not affected by exposure to FeCl$_3$, presumably because the overcoated PDPPT-TT layer minimized the diffusion of FeCl$_3$ into the underlying PMMA layer (fig. S2). In addition, 10 weight % (wt %) azide cross-linker was used to pattern PMMA, which is twice the amount used for cross-linking the polymer semiconductor (5 wt %). This reduced the free volume of the cross-linked PMMA layer and prevented the penetration of the dopant into the PMMA layer. The described patterning and FeCl$_3$ doping processes enabled the successful fabrication of all three electrodes (source, drain, and gate electrodes) simultaneously. Optical microscopy (OM) images of the PTFT in each fabrication step are shown in the lower panel of Fig. 1C.

Characterization of FeCl$_3$-doped semiconducting polymers

High mobility and high electrical conductivity should be the key considerations in the selection of an OSC material for the fabrication of homojunction PTFTs because these factors play a crucial role in the performance of the semiconducting channel and the source/drain electrodes (3, 34, 35). Diketopyrrolopyrrole (DPP)–based polymers are promising candidates for this purpose because of their high charge carrier mobility; specifically, the highly planar structure of a bicyclic lactam ring results in good molecular ordering with efficient charge transport (1, 5, 36, 37). DPP-based polymers have been reported to show high hole mobilities exceeding 1 cm^2 V^{-1} s^{-1} and an interconnected nanofibrillar morphology with an edge-on orientation (36–38). Furthermore, high electrical conductivity can be achieved when provided with sufficient charge carrier concentration together with high carrier mobility. DPP-based polymers have been reported to show an electrical conductivity of 50 to 100 S cm^{-1} upon doping (19, 39). To take advantage of such excellent electrical properties, we selected a p-type π-conjugated polymer, PDPPT-TT, to prepare the semiconducting layer and the source/drain electrodes of the homojunction PTFTs. Figure 2A shows the molecular structure of PDPPT-TT. It was synthesized with a number-average molecular weight of 100 kDa by a modified version of a previously reported synthesis procedure (36, 40). In the doping process, PDPPT-TT (~50 nm thick) films were prepared on glass substrates via spin-coating from chloroform solutions (5 mg ml^{-1}). Then, the pristine PDPPT-TT films were preannealed at 100°C for 10 min before doping. FeCl$_3$ dopant solution in acetonitrile was coated onto the polymer film by spin-coating. Acetonitrile is a semiorthogonal solvent in which a precast polymer film does not dissolve but rather expands, which enables the dopant to penetrate the film without disturbing the ordered polymer packing. The doping level was fine-tuned by optimizing the dopant concentration (0 to 50 mM). Upon doping, FeCl$_3$ removed electrons from the semiconducting polymer to generate positive charge carriers (i.e., positive polarons and bipolarons) along the polymer backbone, which caused the electrical conductivity to improve by several orders of

magnitude (fig. S3) (32, 33, 41). The doping process was confirmed by the acquisition of UV-Vis absorption spectra of the PDPPT-TT film under variation of the concentration of the dopant solution (Fig. 2B). The absorption at λ_{abs} = 811 nm corresponding to a bandgap transition decreased gradually as the dopant concentration increased from 0 to 50 mM. Simultaneously, a broad peak corresponding to mid-gap transitions appeared in the near-infrared (NIR) range over 900 nm, which indicated the generation of polaronic and bipolaronic species. The UV-Vis data therefore demonstrate that the doping level and the resulting conductivity can be controlled by the adjustment of the FeCl$_3$ concentration. The electrical conductivity of the p-doped PDPPT-TT as a function of [FeCl$_3$] was measured by the four-point probe method, as shown in Fig. 2C. As the dopant concentration increased, the electrical conductivity increased from 2.2×10^{-6} (before doping) to 97.0 (±3.8) S cm^{-1} at [FeCl$_3$] of 50 mM. This increase in electrical conductivity via doping was also reflected in the electrical properties of the PTFTs: Transfer characteristics (fig. S4A), hole mobility (fig. S4B), and output characteristics were improved as dopant concentration increased (fig. S5).

The doped PDPPT-TT films with various concentrations of the dopant (FeCl$_3$) were additionally analyzed by grazing-incidence wide-angle x-ray scattering (GIWAXS) and atomic force microscopy (AFM) to investigate their morphological changes. Sequential doping has a great advantage over typical dopant mixing in that it minimizes the disruption of the structure of a crystalline film (42, 43). Figure 2D and fig. S6 present the GIWAXS images of PDPPT-TT films doped with various concentrations of FeCl$_3$ {i.e., [FeCl$_3$] = 0 (pristine), 10, 30, and 50 mM}. The GIWAXS patterns of all the films showed ordered lamellar peaks in the out-of-plane (OOP) direction and a π-π stacking peak in the in-plane (IP) direction, which indicates that the PDPPT-TT film had an edge-on orientation. Figure 2E shows Gaussian-fitted line-cut profiles of the doped PDPPT-TT films. The lamellar spacing and π-π stacking distances did not show any noticeable changes with an increase in [FeCl$_3$] up to 30 mM. This suggests that the dopant mainly penetrated into the amorphous region, and the resulting dopant anions (FeCl$_4^-$) were located mainly near the alkyl side chains; that is, the dopant did not disturb the crystalline polymer packing (fig. S7). At [FeCl$_3$] = 50 mM, slight increases in the lamellar spacing (from 23.92 to 24.54 Å) and π-π stacking distance (from 3.76 to 3.85 Å) were observed (Fig. 2F), but the strong packing structure of the films was still maintained. The detailed packing parameters of the films as extracted from the GIWAXS measurements are listed in table S1. The morphology of the polymer films at various dopant concentrations was visualized by AFM, as shown in fig. S8. The AFM images indicated that an increase in the dopant concentration did not affect the morphology of the films much.

The effect of p-doping on the PDPPT-TT film was further confirmed via the measurement of the surface potential (V_{CPD}) of the semiconducting polymer films with various dopant concentrations by Kelvin probe force microscopy (KPFM). V_{CPD} of the doped PDPPT-TT films gradually decreased with increasing [FeCl$_3$], as indicated by the gradual darkening of the KPFM mapping images in the upper panel of Fig. 2G. In detail, the Gaussian-fitted distribution of the V_{CPD} values (lower panel of Fig. 2G) revealed that V_{CPD} of the pristine film was −0.04 V whereas that of the doped film ([FeCl$_3$] = 50 mM) was −0.38 V. Figure 2H shows the work function of the PDPPT-TT films as a function of [FeCl$_3$]. The work function ($W_{PDPPT-TT}$) of the doped films as calculated using the equation

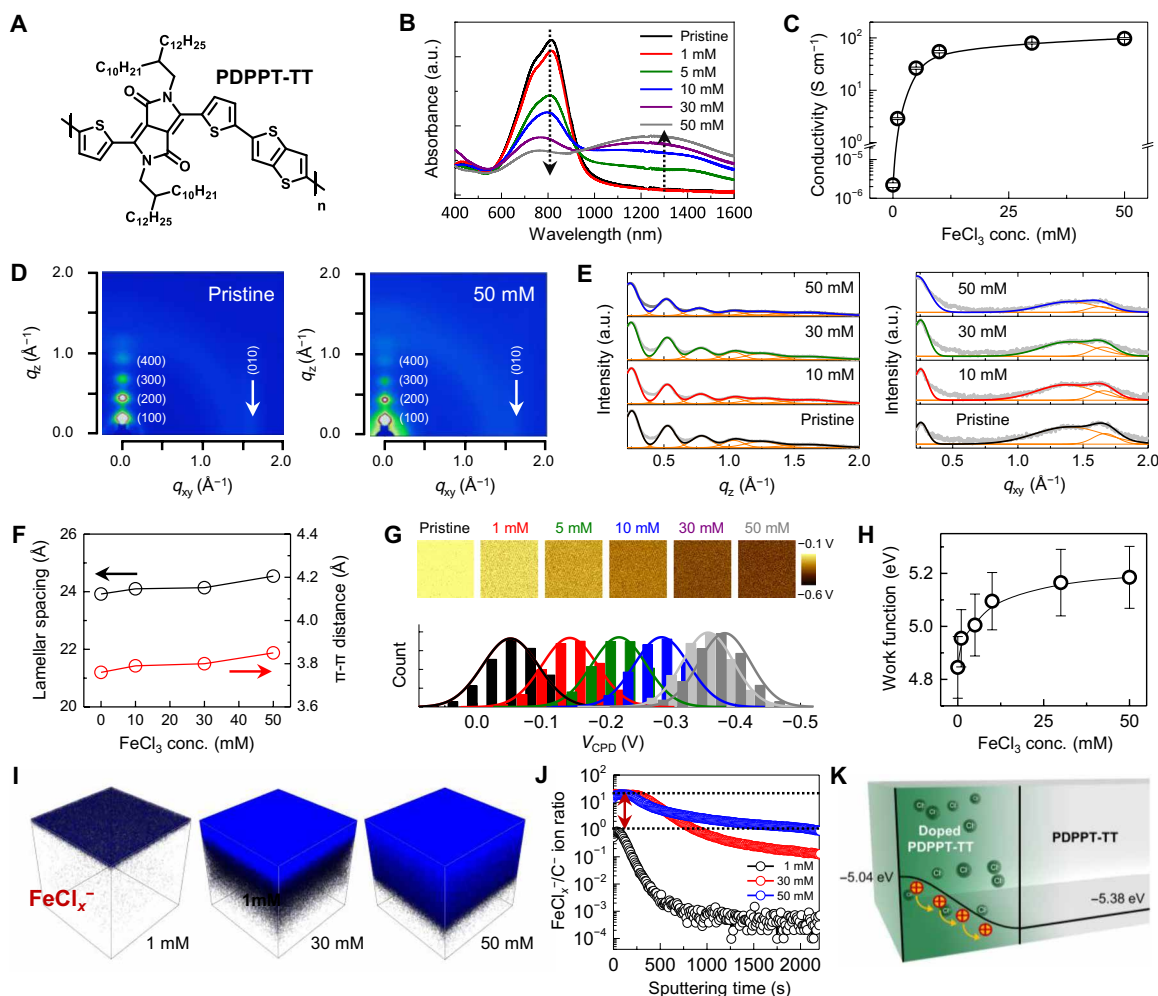**Fig. 2. Characterization of FeCl₃-doped PDPPT-TT.** (**A**) Chemical structure of PDPPT-TT. (**B**) UV-Vis absorption spectra of PDPPT-TT films at various [FeCl₃]. a.u., arbitrary units. (**C**) Electrical conductivity of doped PDPPT-TT films as a function of [FeCl₃]. (**D**) GIWAXS patterns of PDPPT-TT films doped with various concentrations of FeCl₃. (**E**) Line-cut profiles of doped PDPPT-TT films along the OOP and IP directions as a function of [FeCl₃]. (**F**) Lamellar spacing determined from OOP (300) peak and π-π stacking distance determined from IP (010) peak for PDPPT-TT films as a function of doping concentration. (**G**) KPFM images and histograms of surface potentials for PDPPT-TT films doped with various concentrations of FeCl₃. (**H**) Work function of surface of doped PDPPT-TT film as a function of [FeCl₃] (extracted from V_{CPD}). (**I**) TOF-SIMS three-dimensional tomography images of doped PDPPT-TT films at various doping concentrations. (**J**) TOF-SIMS depth profiles (ratio of FeCl$_x^-$ ions to C⁻ ions) of PDPPT-TT films with various dopant concentrations as a function of sputtering time. (**K**) Schematic illustration of gradient injection of carriers for selectively doped PDPPT-TT films.

$eV_{CPD} = W_{probe} - W_{PDPPT-TT}$, where W_{probe} is the work function of the probe tip, showed a notable increase of 0.34 eV (i.e., from 4.84 to 5.18 eV) with an increase in [FeCl₃] from 0 to 50 mM. The diffusion of the FeCl₃ dopant into the PDPPT-TT film was investigated by time-of-flight secondary ion mass spectrometry (TOF-SIMS). As illustrated in Fig. 2I and fig. S9, at a low FeCl₃ concentration, its ions were unevenly distributed throughout the entire polymer film, and they remained mainly near the surface; in contrast, when the FeCl₃ concentration was high, its ions diffused into the polymer film to a sufficient depth and reached its inner part. The TOF-SIMS depth profile was quantitatively illustrated by plotting the ratio of FeCl$_x^-$ to C⁻ ions at various dopant concentrations as a function of the sputtering time, as shown in Fig. 2J. The ion ratio on the surface of the PDPPT-TT film doped with 1 mM FeCl₃ was almost identical to that at the bottom of the film doped with 50 mM FeCl₃, which

indicates that the work function of the latter film gradually decreased from 5.18 to 4.84 eV with an increase in its depth. The gradual change in the work function with the depth in the doped PDPPT-TT film indicates that the highest occupied molecular orbital (HOMO) level bent gradually to align the Fermi level of the upper layer of the electrode with the Fermi level of the semiconductor region (fig. S10). The HOMO level at a sufficient depth in the doped region eventually reached that of the undoped semiconductor region (−5.38 eV, as shown in fig. S11); this consequently caused an enhancement in the efficiency of hole injection into the semiconductor (Fig. 2K). These analysis results suggest that by inducing a gradual change in the work function via the simple sequential doping process, we can fabricate an electrode whose performance is comparable to that of the conventional Au electrode, although its electrical conductivity and work function are lower than that of Au.

Electrical properties of completely foldable homojunction PTFTs and logic circuits

The electrical characteristics of the homojunction p-doped PTFT fabricated as described above were investigated to confirm its function as an electrode. Figure 3A shows representative transfer characteristics [drain current (I_D) versus gate voltage (V_G)] of the PTFT at a fixed drain voltage (V_D) of −60 V. The device exhibited hole-dominant transport behavior. Moreover, negligible current hysteresis was observed between the forward and reverse sweeps because of low charge trap densities at the PDPPT-TT/PMMA interface. Figure 3B shows representative output characteristics (I_D-V_D) of the PTFT at various V_G. The device showed reasonable gate modulation in both the linear regime (at low V_D) and the saturation regime (at high V_D). The electrical properties, i.e., hole mobility (μ), on-off current ratio (I_{on}/I_{off}), and turn-on voltage (V_{on}), of a total of 36 PTFTs are summarized in Fig. 3C. The μ value of the PTFTs

was calculated in the saturation regime according to the equation $I_D = C_S \cdot \mu \cdot W \cdot (V_G − V_{TH})^2 / 2L$ (44, 45), where C_S is the specific capacitance of the cross-linked PMMA gate dielectric (5 nF cm^{-2}), V_{TH} is the threshold voltage, W is the channel width (1000 μm), and L is the channel length (100 μm). The average μ value was 0.71 ($\pm$0.12) cm^2 V^{-1} s^{-1}, the average V_{on} was +10.1 ($\pm$2.0) V, and the average I_{on}/I_{off} was 6.5 ($\pm$1.1) $\times$ 10^5. It should be noted that the electrical properties of the homojunction PTFTs were comparable to those of PTFTs with a Au contact (fig. S12).

The contact properties of the PDPPT-TT TFTs were investigated by measuring their channel length–dependent resistance by the transmission line method (46). Figure 3D shows a schematic of a PTFT with a Au metal contact (top) and a PTFT with a FeCl$_3$-doped polymer contact (bottom). The channel length was varied from 30 to 180 μm, whereas the channel width was fixed at 1000 μm. Figure 3E shows a comparison of the width-normalized total resistance
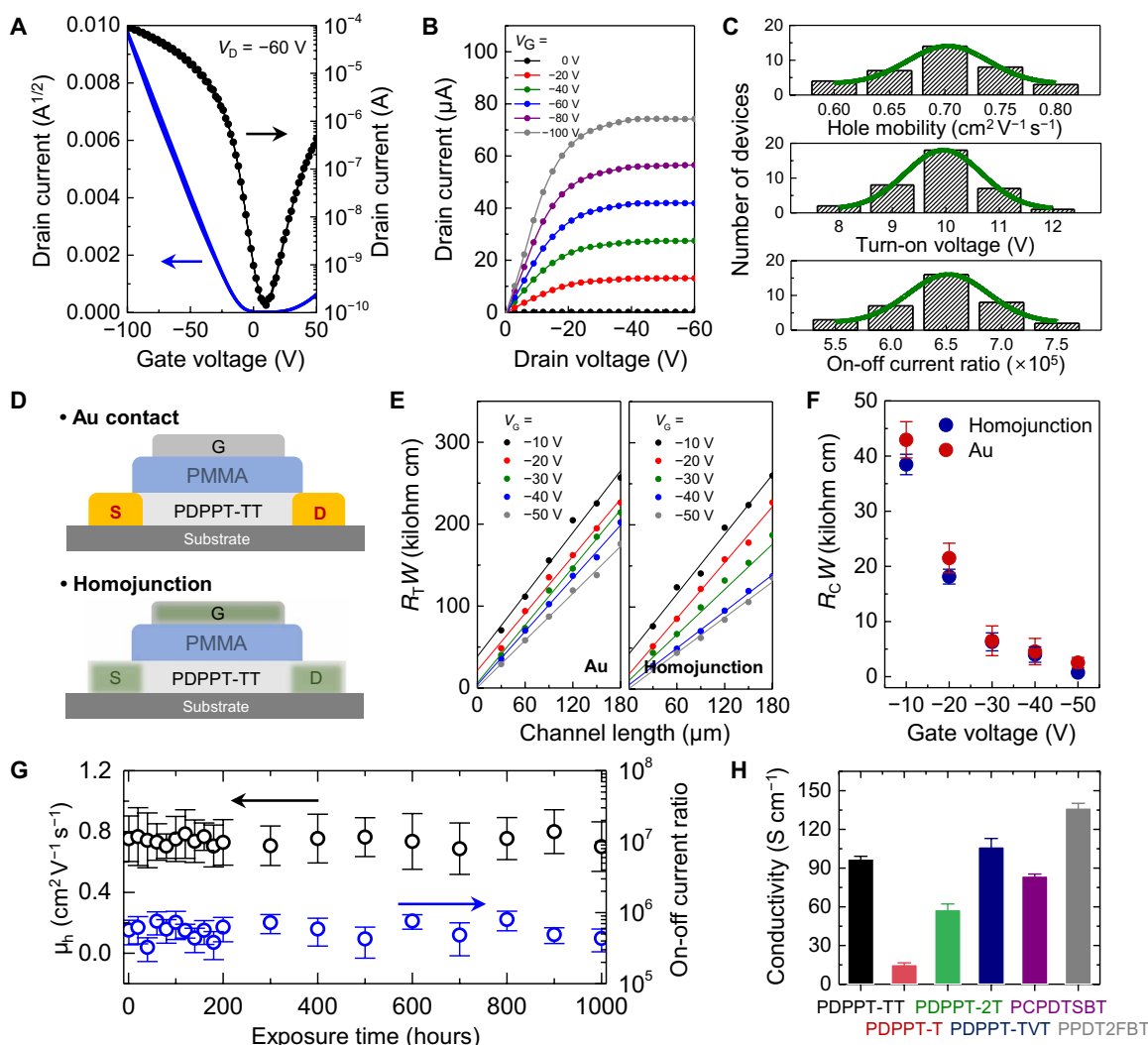

Fig. 3. Electrical properties of homojunction PTFTs. (**A**) Transfer characteristics and (**B**) output characteristics of homojunction PDPPT-TT TFTs. (**C**) Histograms of hole mobility (top), turn-on voltage (middle), and on-off current ratio (bottom) of total 36 PDPPT-TT TFTs. (**D**) Schematic illustration of device structure of PTFTs with conventional Au contact (top) and FeCl$_3$-doped polymer contact (bottom). (**E**) Comparison of width-normalized total resistance (R_TW) of Au contact and FeCl$_3$-doped polymer contact in the V_G range of −10 to −50 V. (**F**) Width-normalized contact resistance (R_CW) as a function of V_G. (**G**) Ambient stability of PTFTs as a function of exposure time. (**H**) Electrical conductivity of various semiconducting polymers doped with 10 to 50 mM FeCl$_3$.

($R_T W$) of the Au contact and the $FeCl_3$-doped polymer contact measured in the V_G range of −10 to −50 V. The contact resistance (R_C) values were determined from the zero-length intersection of the linear fit of $R_T W$, which can be expressed as $R_{CH} L + R_C W$ (where R_T is the total resistance and R_{CH} is the resistance of the semiconducting channel). The width-normalized contact resistance ($R_C W$) was plotted as a function of V_G, as shown in Fig. 3F. As V_G increased from −10 to −50 V, the $R_C W$ of the PTFTs decreased from 38.4 to 0.7 kilohm cm. It should be noted that in the same V_G range, these values were comparable to those of a typical Au-contact transistor. This comparable contact resistance of the PDPPT-TT electrode, despite its conductivity and work function being lower than those of the Au electrode, is ascribed to the promoted charge injection from the source/drain electrodes to the semiconducting channel resulting from the change in the work function with depth (in the doped PDPPT-TT electrode), as discussed earlier. The ambient stability of the PTFTs was also evaluated. As shown in Fig. 3G, both the μ and the I_{on}/I_{off} showed a negligible change even after 1000 hours of exposure to air; this result confirms the stability of the devices in the ambient environment. We presume that the high stability of the devices is probably due to the hindered diffusion of oxygen and water molecules in the cross-linked polymer films and the geometry of PTFTs that encapsulates the semiconducting channel areas. The formation of high-performance electrodes through selective doping could further be extended to various polymer semiconductors (see figs. S13 to S15 and table S2) (33, 41, 47). Figure 3H shows the electrical conductivity of various semiconducting polymers doped with 10 to 50 mM $FeCl_3$. All five polymers showed electrical conductivity in the range of 15 to 119 S cm^{-1}. Figures S16 and S17 show the representative transfer curves and output curves, respectively, of the homojunction PTFTs with the semiconducting polymers at a fixed V_D of −60 V. Table 1 summarizes their corresponding electrical properties. It can be concluded from these results that the approach of selective doping for forming a homojunction is generally applicable to various polymer semiconductors.

The electrical characteristics of the PDPPT-TT–based TFT arrays under extreme bending conditions are shown in Fig. 4, which demonstrate their excellent mechanical stability under these conditions. Specifically, Fig. 4A shows a series of transfer characteristics of a PTFT under different bending strains. The negligible variation in the transfer curves indicates the excellent mechanical stability of the device even after bending at the minimum bending radius of 0.01 mm (the minimum bending radius was confirmed by scanning electron microscopy analysis, as shown in fig. S18). Representative device parameters of the PTFTs, including μ, V_{on}, and I_{on}/I_{off}, were extracted from the transfer curves and plotted as a function of the

bending radius (Fig. 4B). All three parameters remained almost invariant under extreme bending conditions (bending radius = 0.01 mm): Under the bending conditions, μ was 0.78 cm^2 V^{-1} s^{-1}, I_{on}/I_{off} was 3.2 × 10^5, and V_{on} was +13.4 V (compared to the values of 0.81 cm^2 V^{-1} s^{-1}, 3.3 × 10^5, and + 9.8 V, respectively, under the unbent condition). Figure 4C shows photographic images of a PTFT folded parallelly and perpendicularly with respect to the semiconducting channel. The I_D-V_G curves of the device were almost the same for both the folding directions (Fig. 4D). A folding cycle test was also performed to confirm the durability of the PTFTs. As seen in Fig. 4E, there was no noticeable degradation in the electrical properties of the PTFTs up to 2000 folding cycles (the bending radius was 0.01 mm in both folding directions). On the other hand, in the cases of PEDOT:PSS and Au electrode–based PTFTs that have heterojunction interfaces, notable degradations in electrical properties were observed under the same folding conditions, as shown in fig. S19.

From the above discussion, we hypothesized that this excellent mechanical stability of the devices was attributable to a combination of formation of the homojunction at the electrode/semiconductor interface and the enhanced interfacial adhesion resulting from azide cross-linking. To verify this hypothesis, we performed strain-stress measurements of various polymer films by the film-on-water (FOW) method and a peel test (48–50). Figure 4F and fig. S20 show the setup of the FOW test, which enables determining the stress-strain relationship of a pseudo-freestanding polymer thin film floated onto water with high surface tension. Three different samples were tested by this method: (i) a PDPPT-TT film doped with $FeCl_3$ (which contained the homojunction included in the PTFT arrays), (ii) a PDPPT-TT film deposited with Au (which contained the heterojunction included in a typical PTFT with metal electrodes), and (iii) a PDPPT-TT film deposited with a PEDOT:PSS layer to form a polymer-polymer heterojunction. In all three samples, the thickness of the PDPPT-TT layer was fixed at 200 nm. Figure 4G shows the stress-strain relationships of these films measured at a strain rate of 0.5 mm min^{-1}. The tensile modulus of the doped PDPPT-TT film as estimated from the slope of the curve was around 17 times smaller than that of the Au-deposited PDPPT-TT film, which is preferred for deformable devices. The elastic limit and tensile modulus of the films are plotted in Fig. 4H. The elastic limit of the doped PDPPT-TT film could be extended up to a strain of 6.4%, which is higher than the fracture limit of the Au-deposited film (strain of 2.0%; this film was brittle, and no clear transition from the elastic region to the plastic region under tensile stress was observed). These results support the potential of the approach of forming a homojunction between an electrode and a semiconductor for the reliable

Table 1. Summary of electrical characteristics of homojunction PTFTs.

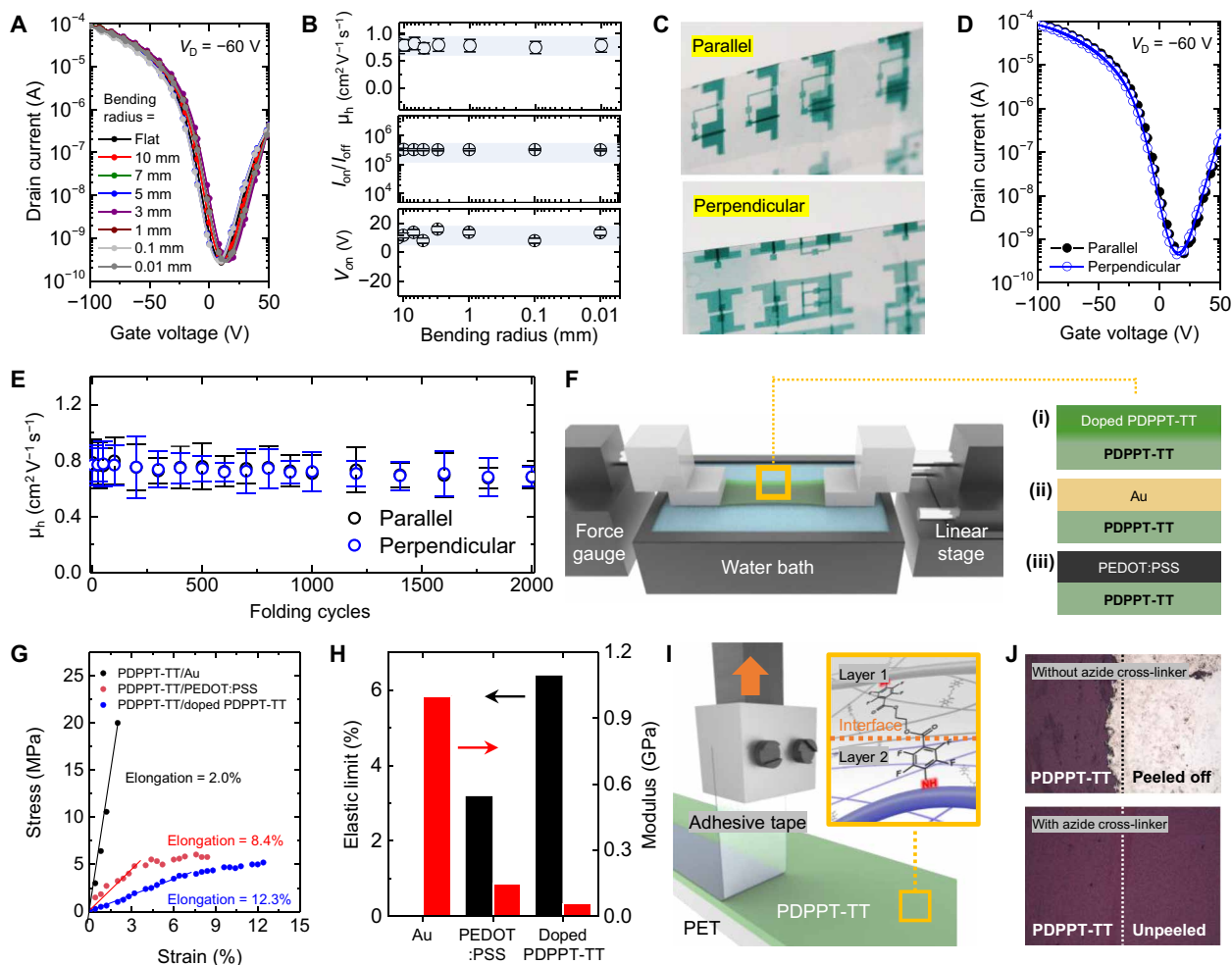| Semiconductor	μ (cm^2 V^{-1} s^{-1})	I_{on}/I_{off}	V_{on} (V)	V_{TH} (V)
PDPPT-TT	0.71 (±0.12)	6.5 (±1.1) × 10^5	+10.1 (±2.0)	−15.6 (±2.1)
PDPPT-T	0.43 (±0.11)	2.1 (±1.0) × 10^5	+6.3 (±2.1)	−21.7 (±2.1)
PDPPT-2T	0.55 (±0.13)	6.0 (±2.1) × 10^5	+6.1 (±4.4)	−20.8 (±2.3)
PDPPT-TVT	0.67 (±0.19)	4.6 (±1.8) × 10^5	+4.2 (±3.8)	−22.8 (±2.1)
PCPDTSBT	0.13 (±0.04)	3.2 (±1.2) × 10^5	+12.3 (±6.2)	−16.3 (±3.3)
PPDT2FBT	0.33 (±0.08)	1.2 (±0.4) × 10^5	+39.8 (±8.1)	−24.3(±4.4)

Fig. 4. Mechanical stability of homojunction PTFTs. (**A**) Transfer characteristics of PTFTs at various bending radii (flat, 10, 7, 5, 3, 1, 0.1, and 0.01 mm). (**B**) Electrical parameters of PTFTs as a function of bending radius. (**C**) Photographic images of PTFT folded parallelly and perpendicularly with respect to semiconducting channel. Photo credit: M. J. Kim (Department of Chemical and Biomolecular Engineering, Yonsei University). (**D**) Transfer characteristics of PTFTs folded in parallel and perpendicular directions. (**E**) Hole mobility of PTFTs as a function of folding cycles. (**F**) Schematic illustration of FOW test. (**G**) Stress-strain curves and (**H**) elastic limit and tensile modulus of three different film samples with homojunction and heterojunction contacts. (**I**) Schematic illustration of peel test of cross-linked and un–cross-linked polymer films on PET substrates. (**J**) OM images of surface of each polymer film after removal of PI tape.

mechanical deformation of electronic devices vis-à-vis the mechanical deformation achievable for devices containing the conventional metal-polymer heterojunction. The values of the tensile modulus and elastic limit achieved for the doped PDPPT-TT film with the homojunction are more suitable for obtaining reliable deformation than those achieved for the PDPPT-TT film deposited with the PEDOT:PSS layer to form a polymer-polymer heterojunction (data in red). Overall, we conclude that the formation of a homojunction between the electrode and the semiconductor plays an important role in enhancing device stability under mechanical deformation. A peel test was also performed to verify the effect of cross-linking on the interfacial adhesion. Figure 4I shows a schematic illustration of the peel test, in which the adhesion of cross-linked and un–cross-linked PDPPT-TT polymer films with azide cross-linker on PET substrates was compared. To quantify adhesion property, universal testing machine measurements were conducted while peeling off the polymer film (14 mm × 30 mm) prepared on a PET substrate at an extension rate of 0.5 mm s^{-1} (fig. S21). The un–cross-linked polymer film started to peel completely from the PET substrate at a peel strength of 0.8 N/14 mm. On the other hand, the cross-linked polymer film did not peel even at the peel strength of 1.57 N/14 mm, which corresponds to the maximum peeling extension (30 mm) in our measurement system. Figure 4J shows OM images of the surface of each polymer film after removal of the polyimide (PI) tape. As can be seen from the images, the un–cross-linked polymer film was entirely removed when the PI tape was peeled off, whereas the cross-linked polymer film remained on the substrate because of the strong adhesion at the interface. These results visually demonstrate that the adhesion between the adjacent layers is enhanced via interfacial cross-linking, which is expected to be another important factor enhancing the mechanical stability and durability of foldable devices under bending.

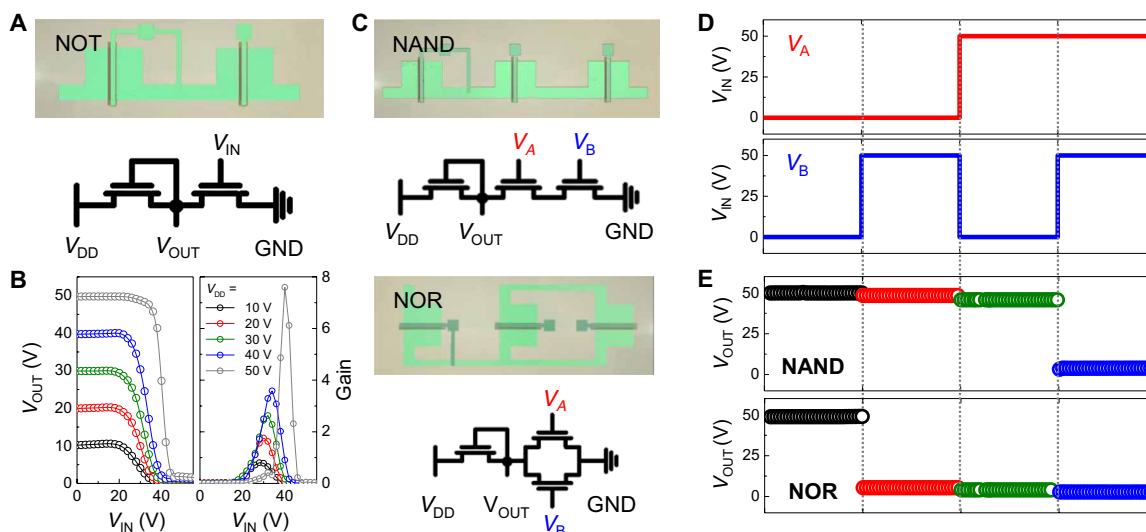Figure 5 shows various logic gates (NOT, NAND, and NOR) fabricated using the homojunction PTFTs. Figure 5A shows an OM

Fig. 5. Electrical characteristics of logic circuits. (**A**) OM image and corresponding schematic circuit diagram of logic circuit for NOT logic gate. GND, ground. (**B**) Voltage transfer curves (left) and signal inverter gain (right) of NOT gate. (**C**) OM image and corresponding schematic circuit diagrams of logic circuits for NAND and NOR logic gates. (**D**) Four possible logic combinations: (0, 0), (1, 0), (0, 1), and (1, 1). (**E**) Output voltages of NAND and NOR gates for the four logic combinations in (D).

image and the corresponding schematic circuit diagram of the logic circuit for the NOT logic gate, which is composed of two PTFTs in series and has a shared output terminal. Figure 5B shows the voltage transfer characteristics of the NOT logic gate at various applied voltages (V_{DD} = 10, 20, 30, 40, and 50 V). The NOT gate showed a typical signal inversion, yielding the logic state "1" for V_{OUT} (V_{OUT} = V_{DD}) when the input voltage was in the logic state "0" (V_{IN} = 0 V). Conversely, the NOT gate yielded the logic state "0" at a higher V_{IN}. The right panel of Fig. 5B shows the calculated signal inverter gain of the NOT logic gate, which is defined as $|dV_{OUT}/dV_{IN}|$. The signal inverter gain of the NOT logic gate was determined to be approximately 7.59 at V_{DD} = 50 V. OM images and the corresponding schematic circuit diagrams of the logic circuits for the NAND and NOR logic gates composed of PTFTs are shown in Fig. 5C. The NAND logic gate is composed of three PTFTs in series, and the NOR logic gate is composed of three PTFTs, two of which are in parallel and connected with the third one in series. Figure 5D shows four possible input logic combinations [(0,0), (1,0), (0,1), and (1,1)] of the two input signals applied to the NAND and NOR logic gates to induce a logic function. The two input voltages (V_{IN}: V_A and V_B) were switched from 0 to 50 V at V_{DD} = 50 V. Figure 5E shows V_{OUT} of the NAND and NOR logic gates for the four different logic combinations applied using the two V_{IN} values. The NAND logic gate yielded the logic state "0" for the input logic combination (1,1) and the logic state "1" for the other three input logic combinations [(0,0), (1,0), and (0,1)]. In contrast, the NOR logic gate yielded the logic state "1" for the input logic combination (0,0) and the logic state "0" for the other three input logic combinations [(1,0), (0,1), and (1,1)]. In addition, the electrical properties of logic circuits were also measured under repeated folding conditions (figs. S22 and S23). No recognizable degradation in the device performance was measured even after up to 2000 folding cycles at an extreme bending radius of 0.01 mm. These experimental results clearly confirm that the NOT, NAND, and NOR logic gates could yield appropriate logic states corresponding to the applied input voltages not only under an unfolded condition but also after repeated foldings.

DISCUSSION

In summary, we successfully fabricated completely foldable homojunction PTFTs by selectively doping a semiconducting polymer film and inducing interfacial cross-linking between adjacent electrical layers. The selective doping process enabled the formation of a homojunction between the semiconducting channel and the source/drain electrodes and therefore enhanced the mechanical stability of the device. The induced cross-linking reaction at the interfaces further improved the mechanical stability. The selective doping also induced a gradual change in the work function with the depth in the electrode region, which contributed to effective charge injection into the semiconductor region. No noticeable degradation in the electrical performance of the resulting PTFTs was observed even after 2000 folding cycles, and superior mechanical stability was confirmed by the FOW and peel tests, compared to conventional PTFTs with metal electrodes. Last, the operation of NOT, NAND, and NOR logic gates composed of the homojunction PTFTs was successfully demonstrated. The concept of doped semiconducting polymer–based homojunction devices presented in this paper is expected to open up new avenues in completely foldable electronics.

MATERIALS AND METHODS
Fabrication of completely foldable PTFTs array

A cleaned 12-μm-thick PET film (Teijin DuPont Films, Mylar 800) by ultrasonication in acetone, isopropanol, and deionized water in sequence for 10 min each was used as a substrate. A glass substrate coated with a 100-μm-thick poly(dimethylsiloxane) (PDMS) (Dow Corning, Sylgard 184) film was used as a supporting carrier substrate for easy handling of the PET substrate. Azide cross-linker (5 wt %) was added to the PDPPT-TT solution, which was prepared by dissolving PDPPT-TT in anhydrous CB at a concentration of 5 mg ml^{-1}. The bottom layer (semiconductor and electrode area) was deposited by spin-coating the mixture solution of PDPPT-TT and azide cross-linker onto the PET substrate at 1000 rpm for 30 s inside a glovebox. The thickness of the resulting polymer film was 52 nm.

Then, the polymer film was exposed to a UV light (wavelength, 254 nm; power, 1000 W cm^{-1}) for 30 s through a shadow mask. After cross-linking, the un–cross-linked area was removed by rinsing with CB solvent, and then the cross-linked polymer film was stored in a glovebox for 4 hours to remove residual solvent. To form a gate dielectric, a mixture solution of PMMA (M_w: 120 kDa; Sigma-Aldrich):azide cross-linker (90:10 wt % in n-butyl acetate, 70 mg ml^{-1}) was spin-coated at 1000 rpm for 1 min followed by sintering in a vacuum oven at 80°C for 6 hours. The thickness of the cross-linked PMMA film was 492 nm. Then, the polymer gate electrode was fabricated by spin-coating the mixture solution of PDPPT-TT and azide onto the cross-linked PMMA layer. The cross-linking of gate dielectric and gate electrode was performed by following the same cross-linking method as described above. Subsequently, a sequential doping of FeCl$_3$ was performed by spin-coating a 50 mM FeCl$_3$ solution in acetonitrile at 2500 rpm for 30 s. Last, the polymer film was dried in a glovebox at 80°C for 1 min. The electrical properties of the PTFTs were measured at room temperature in the dark using a Keithley 4200 semiconductor characterization system.

Characterization

The specific capacitance of the polymer gate dielectric was measured using the Agilent E-4980a inductance-capacitance-resistance (LCR) meter in the frequency range of 100 Hz to 1 MHz. UV-Vis absorption spectra were recorded using the JASCO V-630 spectrophotometer and Cary 6000i UV-Vis-NIR bundle (G9826A). Cyclic voltammetry was obtained using a VersaSTAT3 with a three-electrode cell (platinum electrode coated with an OSC film as a working electrode, platinum wire as a counter electrode, and Ag/Ag$^+$ electrode as a reference electrode) in 0.1 M tetrabutylammonium tetrafluoroborate in acetonitrile at a scan rate of 0.05 V s^{-1}. The electrical conductivity of the doped polymer films was measured by the four-point probe method (Keithley 2634B). The distribution of FeCl$_3$ in the PDPPT-TT film was confirmed by TOF-SIMS (ION-TOF, Germany). Bi^{3+} (30 keV) was used as the primary ion source in TOF-SIMS. The analysis area was 100 μm × 100 μm. Sputter etching of the FeCl$_3$-doped PDPPT-TT film was performed using an Ar gas cluster ion beam with an accelerating voltage of 2.5 keV. KPFM and tapping-mode AFM measurements were performed using the Park Systems NX10 atomic force microscope under ambient conditions. The packing structure of the semiconducting polymer films was investigated by GIWAXS at the 9A beam-line at the Pohang Light Source II, Republic of Korea. The stress-strain curves of the films were obtained by the FOW method using a force gauge (M5-012, Mark-10, USA) and a force measurement test stand (ESM303, Mark-10, USA) at a strain rate of 0.5 mm min^{-1}. An adhesive PDMS layer was exploited to hold the film while applying tensile stress.

SUPPLEMENTARY MATERIALS

Supplementary material for this article is available at http://advances.sciencemag.org/cgi/content/full/7/34/eabg8169/DC1

REFERENCES AND NOTES

1. J. Y. Oh, D. Son, T. Katsumata, Y. Lee, Y. Kim, J. Lopez, H.-C. Wu, J. Kang, J. Park, X. Gu, J. Mun, N. G.-J. Wang, W. Yin, W. Cai, Y. Yun, J. B.-H. Tok, Z. Bao, Stretchable self-healable semiconducting polymer film for active-matrix strain-sensing array. *Sci. Adv.* **5**, eaav3097 (2019).

2. C. Liu, H. Chen, X. Hou, H. Zhang, J. Han, Y.-G. Jiang, X. Zeng, D. W. Zhang, P. Zhou, Small footprint transistor architecture for photoswitching logic and in situ memory. *Nat. Nanotechnol.* **14**, 662–667 (2019).

3. S. Wang, J. Xu, W. Wang, G.-J. N. Wang, R. Rastak, F. Molina-Lopez, J. W. Chung, S. Niu, V. R. Feig, J. Lopez, T. Lei, S.-K. Kwon, Y. Kim, A. M. Foudeh, A. Ehrlich, A. Gasperini, Y. Yun, B. Murmann, J. B.-H. Tok, Z. Bao, Skin electronics from scalable fabrication of an intrinsically stretchable transistor array. *Nature* **555**, 83–88 (2018).

4. D. Li, W. Y. Lai, Y. Z. Zhang, W. Huang, Printable transparent conductive films for flexible electronics. *Adv. Mater.* **30**, 1704738 (2018).

5. J. Xu, H.-C. Wu, C. Zhu, A. Ehrlich, L. Shaw, M. Nikolka, S. Wang, F. Molina-Lopez, X. Gu, S. Luo, D. Zhou, Y.-H. Kim, G.-J. N. Wang, K. Gu, V. R. Feig, S. Chen, Y. Kim, T. Katsumata, Y.-Q. Zheng, H. Yan, J. W. Chung, J. Lopez, B. Murmann, Z. Bao, Multi-scale ordering in highly stretchable polymer semiconducting films. *Nat. Mater.* **18**, 594–601 (2019).

6. J. A. Rogers, T. Someya, Y. Huang, Materials and mechanics for stretchable electronics. *Sci. Adv.* **327**, 1603–1607 (2010).

7. Y. Wang, C. Zhu, R. Pfattner, H. Yan, L. Jin, S. Chen, F. Molina-Lopez, F. Lissel, J. Liu, N. I. Rabiah, Z. Chen, J. W. Chung, C. Linder, M. F. Toney, B. Murmann, Z. Bao, A highly stretchable, transparent, and conductive polymer. *Sci. Adv.* **3**, e1602076 (2017).

8. K. Sim, Z. Rao, H.-J. Kim, A. Thukral, H. Shim, C. Yu, Fully rubbery integrated electronics from high effective mobility intrinsically stretchable semiconductors. *Sci. Adv.* **5**, eaav5749 (2019).

9. B. Wang, A. Thukral, Z. Xie, L. Liu, X. Zhang, W. Huang, X. Yu, C. Yu, T. J. Marks, A. Facchetti, Flexible and stretchable metal oxide nanofiber networks for multimodal and monolithically integrated wearable electronics. *Nat. Commun.* **11**, 1–11 (2020).

10. D. Ji, T. Li, Y. Zou, M. Chu, K. Zhou, J. Liu, G. Tian, Z. Zhang, X. Zhang, L. Li, D. Wu, H. Dong, Q. Miao, H. Fuchs, W. Hu, Copolymer dielectrics with balanced chain-packing density and surface polarity for high-performance flexible organic electronics. *Nat. Commun.* **9**, 2339 (2018).

11. T. Sekitani, U. Zschieschang, H. Klauk, T. Someya, Flexible organic transistors and circuits with extreme bending stability. *Nat. Mater.* **9**, 1015–1022 (2010).

12. M. Kaltenbrunner, T. Sekitani, J. Reeder, T. Yokota, K. Kuribara, T. Tokuhara, M. Drack, R. Schwödiauer, I. Graz, S. Bauer-Gogonea, S. Bauer, T. Someya, An ultra-lightweight design for imperceptible plastic electronics. *Nat. Commun.* **499**, 458–463 (2013).

13. J. Y. Oh, S. Kim, H.-K. Baik, U. Jeong, Conducting polymer dough for deformable electronics. *Adv. Mater.* **28**, 4455–4461 (2016).

14. K.-W. Seo, C. Cho, H.-I. Jang, J. H. Park, J.-Y. Lee, Enhanced bendability of nanostructured metal electrodes: Effect of nanoholes and their arrangement. *Nanoscale* **12**, 12898–12908 (2020).

15. T. Cheng, Y. Zhang, W.-Y. Lai, W. Huang, Stretchable thin-film electrodes for flexible electronics with high deformability and stretchability. *Adv. Mater.* **27**, 3349–3376 (2015).

16. A. Inoue, H. Yuk, B. Lu, X. Zhao, Strong adhesion of wet conducting polymers on diverse surfaces. *Sci. Adv.* **6**, eaay5394 (2020).

17. B. Lu, H. Yuk, S. Lin, N. Jian, K. Qu, J. Xu, X. Zhao, Pure PEDOT:PSS hydrogels. *Nat. Commun.* **10**, 1043 (2019).

18. V. R. Feig, H. Tran, M. Lee, Z. Bao, Mechanically tunable conductive interpenetrating network hydrogels that mimic the elastic moduli of biological tissue. *Nat. Commun.* **9**, 2740 (2018).

19. Y. Karpov, T. Erdmann, I. Raguzin, M. Al-Hussein, M. Binner, U. Lappan, M. Stamm, K. L. Gerasimov, T. Beryozkina, V. Bakulev, D. V. Anokhin, D. A. Ivanov, F. Günther, S. Gemming, G. Seifert, B. Voit, R. Di Pietro, A. Kiriy, High conductivity in molecularly p-doped diketopyrrolopyrrole-based polymer: The impact of a high dopant strength and good structural order. *Adv. Mater.* **28**, 6003–6010 (2016).

20. H. Yuk, B. Lu, S. Lin, K. Qu, J. Xu, J. Luo, X. Zhao, 3D printing of conducting polymers. *Nat. Commun.* **11**, 1604 (2020).

21. H. Sirringhaus, Device physics of solution-processed organic field-effect transistors. *Adv. Mater.* **17**, 2411–2425 (2005).

22. H. Yuk, T. Zhang, S. Lin, G. A. Parada, X. Zhao, Tough bonding of hydrogels to diverse non-porous surfaces. *Nat. Mater.* **15**, 190–196 (2016).

23. L. Ouyang, B. Wei, C.-c. Kuo, S. Pathak, B. Farrell, D. C. Martin, Enhanced PEDOT adhesion on solid substrates with electrografted P(EDOT-NH$_2$). *Sci. Adv.* **3**, e1600448 (2017).

24. J. W. Borchert, B. Peng, F. Letzkus, J. N. Burghartz, P. K. L. Chan, K. Zojer, S. Ludwigs, H. Klauk, Small contact resistance and high-frequency operation of flexible low-voltage inverted coplanar organic transistors. *Nat. Commun.* **10**, 1119 (2019).

25. H.-W. Park, A. Song, D. Choi, H.-J. Kim, J.-Y. Kwon, K.-B. Chung, Enhancement of the device performance and the stability with a homojunction-structured tungsten indium zinc oxide thin film transistor. *Sci. Rep.* **7**, 11634 (2017).

26. S. H. Chae, W. J. Yu, J. J. Bae, D. L. Duong, D. Perello, H. Y. Jeong, Q. H. Ta, T. H. Ly, Q. A. Vu, M. Yun, X. Duan, Y. H. Lee, Transferred wrinkled Al$_2$O$_3$ for highly stretchable and transparent graphene–carbon nanotube transistors. *Nat. Mater.* **12**, 403–409 (2013).

27. F. Xu, M.-Y. Wu, N. S. Safron, S. S. Roy, R. M. Jacobberger, D. J. Bindl, J.-H. Seo, T.-H. Chang, Z. Ma, M. S. Arnold, Highly stretchable carbon nanotube transistors with ion gel gate dielectrics. *Nano Lett.* **14**, 682–686 (2014).

28. Y. Choi, W.-Y. Park, M. S. Kang, G.-R. Yi, J.-Y. Lee, Y.-H. Kim, J. H. Cho, Monolithic metal oxide transistors. *ACS Nano* **9**, 4288–4295 (2015).

29. A. Dathbun, Y. Kim, Y. Choi, J. Sun, S. Kim, B. Kang, M. S. Kang, D. K. Hwang, S. Lee, C. Lee, J. H. Cho, Selectively metallized 2D materials for simple logic devices. *ACS Appl. Mater. Interfaces* **11**, 18571–18579 (2019).

30. M.-H. Ha, J.-K. Choi, B.-M. Park, K.-Y. Han, Highly flexible cover window using ultra-thin glass for foldable displays. *J. Mech. Sci. Technol.* **35**, 661–668 (2021).

31. R.-Q. Png, P.-J. Chia, J.-C. Tang, B. Liu, S. Sivaramakrishnan, M. Zhou, S.-H. Khong, H. S. O. Chan, J. H. Burroughes, L.-L. Chua, R. H. Friend, P. K. H. Ho, High-performance polymer semiconducting heterostructure devices by nitrene-mediated photocrosslinking of alkyl side chains. *Nat. Mater.* **9**, 152–158 (2010).

32. S. Lee, S. Kim, A. Pathak, A. Tripathi, T. Qiao, Y. Lee, H. Lee, H. Y. Woo, Recent progress in organic thermoelectric materials and devices. *Macromol. Res.* **28**, 531–552 (2020).

33. A. Tripathi, Y. Ko, M. Kim, Y. Lee, S. Lee, J. Park, Y.-W. Kwon, J. Kwak, H. Y. Woo, Optimization of thermoelectric properties of polymers by incorporating oligoethylene glycol side chains and sequential solution doping with preannealing treatment. *Macromolecules* **53**, 7063–7072 (2020).

34. X. Xu, Y. Yao, B. Shan, X. Gu, D. Liu, J. Liu, J. Xu, N. Zhao, W. Hu, Q. Miao, Electron mobility exceeding 10 cm^2 V^{-1}s^{-1} and band-like charge transport in solution-processed *n*-channel organic thin-film transistors. *Adv. Mater.* **28**, 5276–5283 (2016).

35. A. F. Paterson, N. D. Treat, W. Zhang, Z. Fei, G. Wyatt-Moon, G. Faber, G. Vourlias, P. A. Patsalas, O. Solomeshch, N. Tessler, M. Heeney, T. D. Anthopoulos, Small molecule/polymer blend organic transistors with hole mobility exceeding 13 cm^2 V^{-1} s^{-1}. *Adv. Mater.* **28**, 7791–7798 (2016).

36. H. Luo, C. Yu, Z. Liu, G. Zhang, H. Geng, Y. Yi, K. Broch, Y. Hu, A. Sadhanala, L. Jiang, P. Qi, Z. Cai, H. Sirringhaus, D. Zhang, Remarkable enhancement of charge carrier mobility of conjugated polymer field-effect transistors upon incorporating an ionic additive. *Sci. Adv.* **2**, e1600076 (2016).

37. M. J. Kim, A.-R. Jung, M. Lee, D. Kim, S. Ro, S.-M. Jin, H. D. Nguyen, J. Yang, K.-K. Lee, E. Lee, M. S. Kang, H. Kim, J.-H. Choi, B. Kim, J. H. Cho, Structure–property relationships of semiconducting polymers for flexible and durable polymer field-effect transistors. *ACS Appl. Mater. Interfaces* **9**, 40503–40515 (2017).

38. M. Nikolka, K. Broch, J. Armitage, D. Hanifi, P. J. Nowack, D. Venkateshvaran, A. Sadhanala, J. Saska, M. Mascal, S.-H. Jung, J. K. Lee, I. McCulloch, A. Salleo, H. Sirringhaus, High-mobility, trap-free charge transport in conjugated polymer diodes. *Nat. Commun.* **10**, 2122 (2019).

39. A. I. Hofmann, R. Kroon, S. Zokaei, E. Järsvall, C. Malacrida, S. Ludwigs, T. Biskup, C. Müller, Chemical doping of conjugated polymers with the strong oxidant magic blue. *Adv. Electron. Mater.* **6**, 2000249 (2020).

40. K. S. Park, J. J. Kwok, R. Dilmurat, G. Qu, P. Kafle, X. Luo, S.-H. Jung, Y. Olivier, J.-K. Lee, J. Mei, D. Beljonne, Y. Diao, Tuning conformation, assembly, and charge transport properties of conjugated polymers by printing flow. *Sci. Adv.* **5**, eaaw7757 (2019).

41. J. Maiz, M. M. Rojo, B. Abad, A. A. Wilson, A. Nogales, D.-A. Borca-Tasciuc, T. Borca-Tasciuc, M. Martín-González, Enhancement of thermoelectric efficiency of doped PCDTBT polymer films. *RSC Adv.* **5**, 66687–66694 (2015).

42. D. T. Scholes, P. Y. Yee, G. R. McKeown, S. Li, H. Kang, J. R. Lindemuth, X. Xia, S. C. King, D. S. Seferos, S. H. Tolbert, Designing conjugated polymers for molecular doping: The roles of crystallinity, swelling, and conductivity in sequentially-doped selenophene-based copolymers. *Chem. Mater.* **31**, 73–82 (2018).

43. D. T. Scholes, P. Y. Yee, J. R. Lindemuth, H. Kang, J. Onorato, R. Ghosh, C. K. Luscombe, F. C. Spano, S. H. Tolbert, B. J. Schwartz, The effects of crystallinity on charge transport and the structure of sequentially processed F4TCNQ-doped conjugated polymer films. *Adv. Funct. Mater.* **27**, 1702654 (2017).

44. J. Zaumseil, H. Sirringhaus, Electron and ambipolar transport in organic field-effect transistors. *Chem. Rev.* **107**, 1296–1323 (2007).

45. H. H. Choi, K. Cho, C. D. Frisbie, H. Sirringhaus, V. Podzorov, Critical assessment of charge mobility extraction in fets. *Nat. Mater.* **17**, 2–7 (2018).

46. T. Uemura, C. Rolin, T.-H. Ke, P. Fesenko, J. Genoe, P. Heremans, J. Takeya, On the extraction of charge carrier mobility in high-mobility organic transistors. *Adv. Mater.* **28**, 151–155 (2016).

47. Y. Lee, J. Park, J. Son, H. Y. Woo, J. Kwak, Degenerately doped semi-crystalline polymers for high performance thermoelectrics. *Adv. Funct. Mater.* , 2006900 (2020).

48. D. Rodriquez, J.-H. Kim, S. E. Root, Z. Fei, P. Boufflet, M. Heeney, T.-S. Kim, D. J. Lipomi, Comparison of methods for determining the mechanical properties of semiconducting polymer films for stretchable electronics. *ACS Appl. Mater. Interfaces* **9**, 8855–8862 (2017).

49. J.-H. Kim, A. Nizami, Y. Hwangbo, B. Jang, H.-J. Lee, C.-S. Woo, S. Hyun, T.-S. Kim, Tensile testing of ultra-thin films on water surface. *Nat. Commun.* **4**, 2520 (2013).

50. D. Wirthl, R. Pichler, M. Drack, G. Kettlguber, R. Moser, R. Gerstmayr, F. Hartmann, E. Bradt, R. Kaltseis, C. M. Siket, S. E. Schausberger, S. Hild, S. Bauer, M. Kaltenbrunner, Instant tough bonding of hydrogels for soft machines and electronics. *Sci. Adv.* **3**, e1700053 (2017).